Chapter 2

Cylindrical Nearfield Acoustical Holography

MATTEO KIRCHNER [1,2,3]*, EUGÈNE NIJMAN* [2]

[1] *KU LEUVEN, DEPARTMENT OF MECHANICAL ENGINEERING*
[2] *VIRTUAL VEHICLE RESEARCH CENTER*
[3] *MEMBER OF FLANDERS MAKE*

1 EXECUTIVE SUMMARY

Automotive industry is asking for new methodologies to characterise the acoustic emissions of electric motors, since their integration in electric vehicles and plug-in-hybrid vehicles is growing.

This chapter presents some research developments of Nearfield Acoustical Holography (NAH) in cylindrical coordinates. In fact, this experimental technique is well suited for the characterisation of acoustic sources such as electric motors.

The theory behind cylindrical NAH is briefly outlined here. A possible limitation of NAH is the need of an overwhelming amount of microphones in the high frequency range, governed by the Nyquist-Shannon sampling theorem. A possible approach to reduce the number of sensors is the so-called compressive sensing. Its formulation, theoretical background and applicability are discussed.

Two numerical test cases are developed to support the theory. First, practical aspects of the classical NAH such as microphone positioning error, measurement noise, hologram distance and measurement aperture are investigated and discussed. Moreover, a second test case helps to understand the applicability of compressive sensing to NAH.

2 INTRODUCTION AND GENERAL FRAMEWORK

Automotive industry is increasingly driven by the need to offer fuel efficient and eco-friendly mobility. In fact, legislators are reducing carbon dioxide limits in order to reach the targets set by international agreements. At the same time, customers are asking for comfortable and innovative vehicles.

The reduction of fuel consumption and pollution is mainly achievable by lightweight

design, downsizing internal combustion engines (ICEs), and through electrification and hybridisation of the vehicle's powertrain.

Unfortunately, these new measures motived by the pressure to lower both the exhaust emission levels and the fuel consumption present new design challenges in the vehicle design process. For example, downsizing conventional ICEs leading to higher vibration levels due to the reduced number of cylinders.

Moreover, under some powering strategies (such as parallel hybrid) multiple propulsion systems are asked to operate automatically according to the driving conditions, with important NVH issues linked to the switch from one configuration to another. For other typologies, an ICE works as range extender, generating a constant noise and vibration level that does not depend on the driving speed, which may be annoying for the driver and the other vehicle occupants.

Pure electric driving is known to produce a low overall noise level, but a tonal component generated by the electric motor(s) may dominate the sound emission and be annoying. Furthermore, secondary noise components such as wind, tire-road friction and powertrain become audible.

Finally, the global noise reduction raises the well-known security issues regarding low-speed traffic such as pedestrians and cyclists.

In this framework, it is clear that automotive industry is asking for new methodologies to characterise the acoustic emissions of electric components. This chapter focuses on an experimental methodology to characterise the noise emissions of an electric motor, based on Nearfield Acoustical Holography (NAH) in cylindrical coordinates. This technique allows the evaluation of sound intensity, as well as pressure level and particle velocity. It is suitable for any type of electric motor without knowing either the internal geometry or the material properties.

This chapter is divided in two parts. The first part (sections 3–4) is theoretical, with section 3 discussing the classical NAH approach in cylindrical coordinates, together with a regularisation procedure to limit the influence of noise. Next, section 4 introduces compressive sensing as a possible way to limit the number of measurements which are required by the classical NAH in the high frequency range. The feasibility of this approach is also taken under consideration.

The second part of this chapter (sections 5–6) presents a few numerical experiments. Section 5 focuses on simulations to understand some practical aspects to be taken into account while performing NAH in cylindrical coordinates. Section 6 shows and discusses a simple test case in which compressive sensing is applied to NAH. Finally, section 7 summarizes the conclusions.

3 CYLINDRICAL NAH

Nearfield Acoustical Holography (NAH) is an experimental technique that allows an accurate characterisation of a source through the inverse propagation of a hologram. NAH is described exhaustively in a book by Earl G. Williams [1], were formulas are given for planar, cylindrical and spherical geometries.

NAH in cylindrical coordinates is extremely well suited for cylindrical sources like electric motors. This section follows the research stream first proposed in [2] and subsequently documented in [3]. First, subsection 3.1 outlines the classical cylindrical NAH, while section 5 will show a numerical test case, which presents a different geometry as well as different parameters if compared to references [2, 3].

3.1 Problem formulation and solution regularisation

Cylindrical Nearfield Acoustical Holography consists in four steps. First, pressure measurements (or alternatively particle velocity measurements [4, 5]) are acquired on a grid of points on a cylindrical surface (the hologram lattice). The second step involves the computation of the angular spectrum through a spatial transform, which gives a wavenumber space (k-space) description of the original distribution. Furthermore, this angular spectrum is multiplied by an inverse propagator for the reconstruction of the pressure or velocity distribution on the target surface. If the target surface corresponds to the source surface, the source velocity distribution may be obtained. Finally, the results are transformed back to the real space.

The NAH procedure may be rewritten as an inverse problem, which is likely to be mathematical ill-posed. The reason why NAH is prone to instability can be found in the distinction between evanescent and non-evanescent waves, and their way of propagating in a medium. Evanescent waves decay exponentially or follow power law decay, depending on the geometry (planar, cylindrical, spherical). Those behaviours lead to an ill-posed inverse problem, where they turn into exponential-like amplifications causing the blowing up of the measurement noise. Several regularisation methods are available to deal with such problem [6, 7, 8, 9], and Tikhonov regularisation has been chosen here.

NAH can be formulated as a single matrix expression. First, let us consider the forward problem shown in eqs. (2.1–2.2) [9], where p is the spatial pressure distribution at a given frequency and w is the velocity distribution on the source. Matrix H is built from a diagonal matrix G containing the direct propagators of each k-space component, pre-multiplied by an inverse DFT matrix F^{-1}, and post-multiplied by F.

$$p = Hw \tag{2.1}$$

$$H = F^{-1}GF \tag{2.2}$$

The inverse problem is shown in eqs. (2.3–2.4), where R_β is the Tikhonov regularised inverse, which depends on the regularisation parameter β. Superscript H denotes the Hermitian matrix (*i.e.*, the conjugate transpose). Note that if $\beta = 0$ (no regularisation), R_β is simply the pseudo-inverse of H.

$$w = R_\beta p \tag{2.3}$$

$$R_\alpha = (H^H H + \beta I)^{-1} H^H \tag{2.4}$$

For increasing β, Tikhonov regularisation progressively reduces the impact of the singular values, starting from the smallest ones. For this reason, it behaves as a low-pass filtering in k-space.

Among the several methods to seek the value of β that best regularises R_β [6, 9], the generalized cross validation (GCV) offers a way to get to a very accurate solution without the need to know the variance of the noise of the system [9].

The GCV imposes to minimize a functional [8], and it is referred to as "the leaving-one-out method", *i.e.*, one measurement point at a time is omitted from the NAH procedure and used as a reference. The optimal β yields the best reconstruction in the omitted points in a least mean square sense [8].

The straightforward implementation of the functional suggested in [8] leads to a very high computational effort. A much more time-efficient algorithm is described in [9].

It is important to emphasize that the GCV scheme is not able to stabilize the problem if the noise components are highly correlated [6].

It is worth to notice that the k-space components are obtained by a two-dimensional discrete Fourier transform (2D-DFT). The sensor spacing is thus governed by the Nyquist-Shannon sampling theorem, leading to an overwhelming amount of transducers in the high frequency range, limiting the practical application of NAH.

4 NAH WITH COMPRESSIVE SENSING

Promising results have been published with regard to compressive sensing (CS) applied to NAH with the aim to reduce the number of microphones without affecting the quality of the reconstruction [10]. Compressive sensing is a well known scheme in the field of audio and image processing, and it allows to slim down data at the source. CS wants to directly acquire the minimum amount of data which is needed to fully represent a signal. In some fields such as digital photography a huge amoutn of data is acquired and immediately compressed in order to fit in a storage drive.

Compressive sensing is based on a concept referred to as signal sparsity, *i.e.*, a signal can be represented (fully or in an approximate way) by just a few components belonging to a certain transformed space. This space is referred to as dictionary, and its components are the so-called basis functions.

Signals are compressible, *i.e.*, they are well approximated by sparse representations, when they have a sparse representation in some domain [11, 12, 13]. The problem is then to represent a signal in that specific domain and keep only the relevant non-zero elements (the sparsest the solution, the better the compression). A simple overview on compressive sensing can be found in [13].

Most of the material regarding the application of compressive sensing to NAH comes from reference [14], and the reader can refer to it for further details. A brief overview can be found also in [3], without any numerical example.

4.1 Problem formulation

According to the notation that has already been introduced while describing the classical NAH procedure in section 3, this subsection deals with the formulation of holography with compressive sensing, highlighting its structure and complexity in comparison to eq. (2.1).

Formally, the only difference is in the definition of the source velocity distribution w, which is shown in eq. (2.5).

$$w = D\alpha \tag{2.5}$$

Matrix D is a dictionary of basis functions and α is a complex column vector containing the coefficients of those basis functions. Dictionaries may be overcomplete [15], meaning that the signal description expressed by eq. (2.5) is not unique, *i.e.*, one basis function can be represented by other basis functions. Mathematically, this corresponds to a non-orthogonal dictionary. Such characteristic can result from either the fact that a dictionary has been designed that way, or because some orthogonal dictionaries (complete dictionaries) are merged together [15].

There are many existing candidates for the composition of a dictionary for compressing sensing, such as Fourier basis functions, wavelets, chirplets [10]. The crucial point is that the

dictionary has to be able to *sparsify* the signal, *i.e.*, only a few atoms should (fully or in an approximate way) describe the signal.

A first step towards the formulation of NAH with compressive sensing can be obtained by substituting eqs. (2.2) and (2.5) in (2.1), resulting in eq. (2.6). It will become clear later that matrix F^{-1} cannot be obtained by matrix inversion. For this reason, eq. (2.6) is rewritten as shown by eq. (2.7), which is discussed in the upcoming list.

$$p = F^{-1}GFD\alpha \tag{2.6}$$

$$p = F_{inv}GFD\alpha \tag{2.7}$$

- $p \in \mathbb{R}^{m\times 1}$ contains the measurements, sampled in space. It consist of complex numbers, since each measurement point carries the frequency domain information at a frequency step. The measurement points may or may not be regularly spaced. A randomly spaced hologram helps to capture the high frequency information with fewer measurements in comparison to the number imposed by the Nyquist-Shannon sampling theorem [10].

- $\alpha \in \mathbb{R}^{n\times 1}$ carries the complex coefficients of the basis functions. It should be as sparse as possible, in order to allow fewer measurement points in comparison with classical holography [12, 11].

- $D \in \mathbb{R}^{l\times n}$ is the dictionary. Its columns are the n basis functions (atoms). Each basis function is evaluated on a set of l regularly spaced points. The choice of l determines the number of spatial Fourier components that will be propagated through G. The finer the sampling, the higher the number of (evanescent) components taken into account.

- $F \in \mathbb{R}^{l\times l}$ is a square matrix that applies the two-dimensional discrete Fourier transform (2D-DFT) to the basis functions.

- $G \in \mathbb{R}^{l\times l}$ has the same size of F. It is a diagonal matrix containing the (complex) propagators related to the corresponding Fourier components. The propagators are defined here for the forward problem (exterior problem), *i.e.*, the propagation goes from the source to the (cylindrical) surface on which the hologram is located.

- $F_{inv} \in \mathbb{R}^{m\times l}$ can not be computed by inverting F, as it was in eqs. (2.2) and (2.6). This is because it may not be square (typically, $m < l$). Moreover, it may be evaluated on a set of randomly spaced points, accordingly to the m measurement positions.

Eq. (2.7) can be written in the compact version shown by eq. (2.8), where A is the so-called global sensing matrix, defined in eq. (2.9). This formulation highlights the measurements vector p, the (sparse) complex coefficients vector α, and matrix A between them.

$$p = A\alpha \tag{2.8}$$

$$A = F_{inv}GFD \tag{2.9}$$

Since the general aim of compressive sensing is to reduce the number of measurement points, there will always be more basis functions than measurement points, *i.e.*, $n > m$.

Consequently, the system described by eqs. (2.8–2.9) is underdetermined, *i.e.*, there are there are fewer equations (measurement points) than unknowns (basis functions).

In order to reconstruct the signal, eq. (2.8) has to be inverted and computed. The solution has then to be insert into eq. (2.5) to obtain the velocity distribution.

Among the infinite number of solutions that an underdetermined system such as eq. (2.8) has, the sparsest solution is the best candidate for the success of compressive sensing. The common Moore-Penrose pseudo-inverse (which relies on a ℓ_2 norm optimisation, *i.e.*, on the least mean square error) does not address this specification [11].

Given an arbitrary underdetermined system such as eq. (2.8), the sparsest among all possible solutions is obtained by a minimization of the ℓ_0 norm of the vector α [16], as shown in eq. (2.10).

$$\min_{\alpha} ||\alpha||_{\ell_0} \;\; subject\ to\ A\alpha = p \tag{2.10}$$

Unfortunately, there are no efficient algorithms to solve such problem, due to the non-convexity of the ℓ_0 norm optimisation [17, 16]. Fortunately, those limitations can be overcome by "relaxing" the ℓ_0 norm up to an ℓ_1 norm problem [18, 19], for the solution of which some methods are available [15].

The so-called basis pursuit (BP) has recently been strongly developed. BP is capable to find the sparsest solution within an overcomplete (non-orthogonal) dictionary [15, 20], while other methods need the basis functions to be orthogonal. Moreover, BP is based on global optimisation, offers better sparsity and stable superresolution, and can be used with noisy data [15].

Under some conditions, which will be discussed in section 4.2, both the ℓ_0 and ℓ_1 problems are proven to give the same and unique result. The relaxation from ℓ_0 norm to ℓ_1 norm of eq. (2.10) leads to the new problem described by eq. (2.11), the solution of which will be sought through a basis pursuit algorithm [15].

$$\min_{\alpha} ||\alpha||_{\ell_1} \;\; subject\ to\ A\alpha = p \tag{2.11}$$

In case of solution approximation, regularisation and noise filtering, a slightly different approach is known as basis pursuit denoising (BPDN) [15].

In the next section, the applicability of the methodology that has been presented up to here will be discussed.

4.2 Feasibility

Since the publication of the first milestones regarding compressive sensing by Donoho [18] and by Candès, Romberg and Tao [21, 17], a huge amount of literature can be found. Some papers are written by the same authors and include a few extensions of the already mentioned references (*e.g.*, [12, 22]), while other researchers applied the theory to image compression, which seems to be the most interested field of application.

In order to get the correct results of eq. (2.10) through the solution of eq. (2.11), having few measurement points and few non-zero basis functions, the matrices of the undetermined system have to satisfy a condition known as restricted isometry property (RIP) [16]. The RIP characterises matrices which are nearly orthonormal, at least when operating on sparse vectors.

After defining the RIP (subsection 4.2.1), it will be explained in subsection 4.2.2 that unfortunately it cannot be satisfied when performing NAH.

4.2.1 The restricted isometry property (RIP)

Let us consider the linear system described by eq. (2.8) and the ℓ_1 problem described by eq. (2.11). The restricted isometry property is a matrix condition which is set by means of some *restricted isometry constants*, defined as the smallest number δ_S such that eq.(2.12) holds for all S-sparse vectors ($S \leq K$, so that δ_S is defined for every $S = 1, 2, \ldots, K$) [22]. A vector is said to be S-sparse if it has at most S nonzero entries.

$$1 - \delta_S \;\leq\; \frac{\|A\alpha\|_{\ell_2}^2}{\|\alpha\|_{\ell_2}^2} \;\leq\; 1 + \delta_S \tag{2.12}$$

Saying that a matrix A satisfies a certain RIP means that for any arbitrary vector α having $S \leq K$ nonzero entries, the result of eq. (2.12) stays confined in a certain band. In other words, there is a certain sparsity K below which the amplification introduced by the matrix transformation remains bounded.

Starting from this definition of RIP, reference [22] states that:

- if $\delta_{2S} < 1$, the ℓ_0 problem of eq. (2.10) has a unique S-sparse solution, *i.e.*, if one can prove that for a certain level of sparsity S any vector α with sparsity up to $2S$ will amplify the matrix $[A]$ less than a factor of 1 (when normalized by $\|\alpha\|_{\ell_2}^2$), there is a unique solution with sparsity S.

- if $\delta_{2S} < \sqrt{2} - 1$, the solution to the ℓ_1 problem of eq. (2.11) is that of the ℓ_0 problem of eq. (2.10), and the convex relaxation is exact, *i.e.*, if one can prove that for a certain sparsity S any vector α with sparsity up to $2S$ will amplify the matrix $[A]$ less than a factor of $\sqrt{2} - 1$ (when normalized by $\|\alpha\|_{\ell_2}^2$), then the solution of the ℓ_1 problem corresponds to the sparsest solution that the ℓ_0 problem would give.

The condition $\delta_{2S} < \sqrt{2} - 1$ corresponds to having the RIP satisfied (*i.e.*, the RIP condition holds) [12].

The definition of RIP paved the way to further studies about the required number of measurements and possible way to enhance the RIP. Reference [12] proposes a formula for the required number of measurements, depending on the sparsity level. If this formula is satisfied and if the global sensing matrix A is a Gaussian random matrix, then it is highly possible that the RIP is satisfied. This implies an *a priori* knowledge of the signal, which may be problematic for the characterisation of an unknown source.

It is then extremely important to find a dictionary which sufficiently sparsifies the signal. It must be underlined that this might not be trivial, especially for NAH applications, since the velocity field may be unknown.

Some attempts to improve the RIP involve dictionary learning [23, 24, 25] and the so-called measurement matrix (also referred to as sensing matrix) [11, 26]. In order to go beyond the Nyquist-Shannon limit, measurement have to carry the high frequency information. This can be achieved substituting the classical regular sampling with a random sampling (in space for images, in time for time-signals) [10].

Please note that both a random measurement matrix and a low matrix coherence are not sufficient conditions to have the RIP satisfied, *i.e.*, they are just tools to enhance (but not guarantee) the RIP.

4.2.2 RIP with Holography

In this paragraph, it will be shown that for acoustical holography it is not possible to satisfy the RIP. The main reason for this has to be found in the matrix G containing the propagators, already introduced in eq. (2.2). Before dealing with this crucial issue, a simplified problem is introduced.

Eq. (2.7) can be rewritten in a simplified version if D is a Fourier dictionary, such that eq. (2.13) applies. Dimensions n and l are the same, *i.e.*, the number of basis functions is equal to the number of the Fourier components.

$$FD = I \tag{2.13}$$

The original signal must contain only a few Fourier components, so that α can be sparse. Accordingly, eqs. (2.7–2.9) become as shown in eqs. (2.14–2.16). Σ replaces then A for the simplified situation set by eq. (2.13).

$$p = F_{inv} G \alpha \tag{2.14}$$

$$p = \Sigma \alpha \tag{2.15}$$

$$\Sigma = F_{inv} G \tag{2.16}$$

Let us first focus on G, which is a square diagonal matrix containing the velocity propagators (g_v) of each wavenumber component. Their formula is presented in eq. (2.17) for a cylindrical geometry [1], where j is the complex variable, Z_0 is the acoustic impedance of the medium (*e.g.*, air), k_0 is the wavenumber of the medium at a given frequency, H_n is the Hankel function of the n^{th} circumferential order, H_n^I is the first derivative of H_n, k_r is defined through k_0 and the longitudinal wavenumber (k_z) as follows: $k_r = \sqrt{k_0^2 - k_z^2}$, r_h is the radius of the cylindrical measurement surface (hologram), and finally a is the radius of the cylindrical source. The hologram distance is then $d = r_h - a$.

$$g_v = \frac{j Z_0 k_0 H_n (k_r r_h)}{k_r H_n^I (k_r a)} \tag{2.17}$$

Fig. 2.1 shows the propagators as a function of the circumferential order, *i.e.*, the circumferential wavenumber (k_θ) multiplied by the source radius a. The propagators have been evaluated for a simple one-dimensional case corresponding to an infinite cylinder ($k_z = 0$ such that $k_r = k_0$), for hologram distances from $d = 0$ m to $d = 0.2$ m and step 0.05 m. The graph refers to a source with radius $a = 0.1$ m radiating in air at a frequency $f = 5000$ Hz.

It can be seen that as d assumes higher values, a different amplification is given to propagating and evanescent components (low and high circumferential orders, respectively).

Having clarified the structure of G, it should now be easy to understand that a good RIP cannot be obtained, not even pre-multiplying it by a random matrix. The difference in the amplification of the k-space components precludes the restricted isometry constants to stay within the RIP limits (*i.e.*, $\delta_{2S} < \sqrt{2} - 1$).

Let us now move on to F_{inv}, which represents an inverse two-dimensional Fourier transform evaluated at the measurement points. Its elements $f_{inv}(k, n)$ assume the formula shown in eq. (2.18), where k and n refer to the measurement position and the Fourier component, respectively.

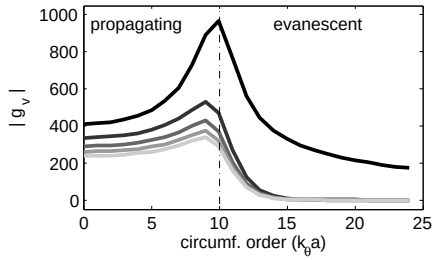

Figure 2.1: $|\, g_v \,|$ in air for $f = 5000$ Hz and $a = 0.1$ m. The colour shade gets lighter while d increases from 0 to 0.2 m, and step 0.05 m.

$$f_{inv}(k, n) = e^{+j2\pi kn} \tag{2.18}$$

The real and imaginary part of $f_{inv}(k, n)$ oscillate according to k and n, but its absolute value is constant for every combination (k, n). In such scenario, a random microphone positioning cannot create a Gaussian random matrix A (or Σ), which would most likely satisfy the RIP.

Thus, for NAH applications it is not possible to increase the rate of success of the basis pursuit algorithm just by randomizing the microphone positions, because of the structure of the matrices. This randomization is only needed to include information about higher frequency components, which cannot be captured by a regular lattice due to the Nyquist-Shannon limit.

5 CYLINDRICAL NAH: NUMERICAL EXPERIMENTS

This section presents a set of numerical experiments to investigate practical aspects of cylindrical holography such as microphone positioning error, background noise and measurement aperture. This section follows the procedure proposed in [2], adapting it for a different geometry as well as different settings.

5.1 Test case

The test case presented in this subsection involves a cylindrical source of length $l = 0.24$ m and radius $a = 0.1$ m, being a representative size for automotive applications such as electric traction motors for green mobility.

A set of acoustical monopoles which are positioned on a cylindrical grid inside a virtual source surface (Fig. 2.2), consisting of a superellipsoid with smooth, almost cylindrical shape. The volume velocity distribution of the monopoles was chosen in order to obtain the frequency independent source surface velocity distribution presented in Fig. 2.3. In order to do so the source simulation technique (SST) [27] was used. The sound pressure in any position of the radiated field can be obtained by straightforward superposition of the monopole fields.

Fig. 2.4 shows the hologram lattice, on which the sound pressures are measured. Unless otherwise stated, the length of the hologram is set to 1.5 times the length of the source, and the distance from the hologram to the surface of the source is $d = 0.04$ m. Moreover, the spatial

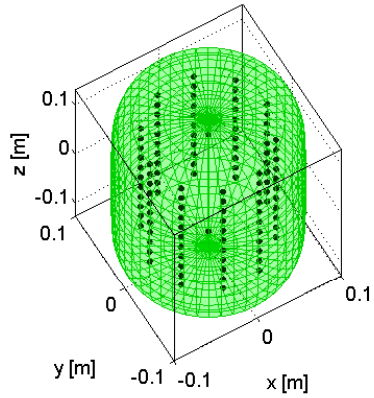

Figure 2.2: Source layout. Virtual source geometry (green surface) and acoustic monopoles for the source simulation technique (black dots).

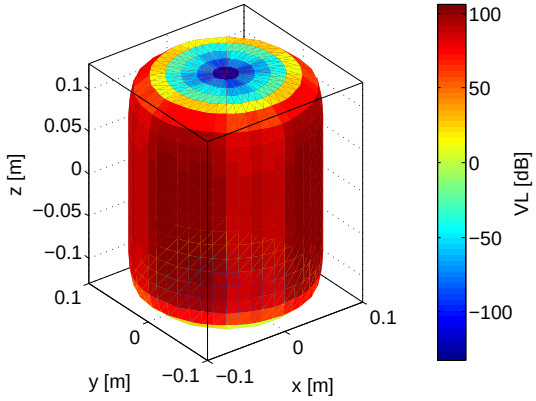

Figure 2.3: Frequency independent target normal velocity level (VL) for the source simulation technique (SST).

sampling is chosen in such a way that the unwrapped mesh presents a similar microphone spacing in the two directions (longitudinal and circumferential sampling $\Delta \approx 0.05$ m). Under these spatial sampling conditions, the frequency limit set by the Shannon sampling theorem is $f = \frac{c_0}{2\Delta} \approx 3430$ Hz (in air, where the speed of sound is $c_0 \approx 343 m/s$).

A finer lattice can be designed if higher frequencies have to be taken into account. However, increasing the amount of microphones may modify the sound field around the source (because of the wave-microphone interaction). Moreover, the data acquisition system may become much more expensive due to the higher number of channels required.

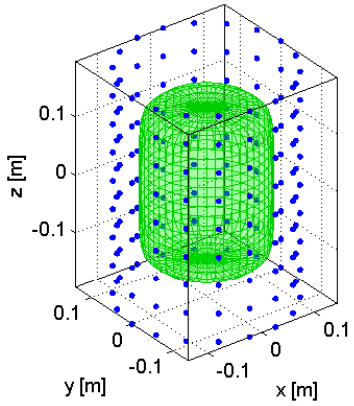

Figure 2.4. Source geometry (green surface) and hologram (blue dots).

5.2 Effects of the regularisation

To show the effects of the regularisation, a small error of zero mean and standard deviation $\sigma = 0.25$ dB was added to the simulations. Fig. 2.5 shows the effect of the regularisation procedure on the surface velocity reconstruction along the z axis at $\theta = 0.35$ rad and along the circumference at $z = 0$ m. The graphs include the reference velocity distribution generated by the acoustic monopoles (solid gray), and the NAH result with and without regularisation (dashed green and dotted blue, respectively). The velocity level is expressed in dB as $VL = 10{\cdot}\log_{10}(\frac{v^2}{v_{ref}^2})$, with $v_{ref} = 5{\cdot}10^{-8}$ m/s.

The results obtained without regularisation are far from being accurate, while the situation completely changes with the regularisation. In particular, a good reconstruction of the velocity distribution is observed in the region of the source (between the vertical dotted black lines in Fig. 2.5).

Fig. 2.6 shows the spatial averaged square error (ε) of the hologram portion corresponding to the source, for a frequency range from 10 to 3410 Hz, and step 100 Hz. Variable ε is defined in eq. (2.19), where v_0 represents the actual source velocity. The bar indicates spatial average.

$$\varepsilon = 10{\cdot}\log_{10}\left(\frac{\bar{v^2}}{\bar{v_0^2}}\right) \tag{2.19}$$

At high frequencies the k-space components exceed the noise and regularisation is not necessary, while at low frequencies the low-pass k-space filter introduced by the regularisation is absolutely necessary and gives excellent results.

5.3 Simulations

5.3.1 Hologram length

For cylindrical NAH, an ideal example that lacks any noise cannot be considered due to the spectral leakage in the longitudinal direction, along which the system is not periodic.

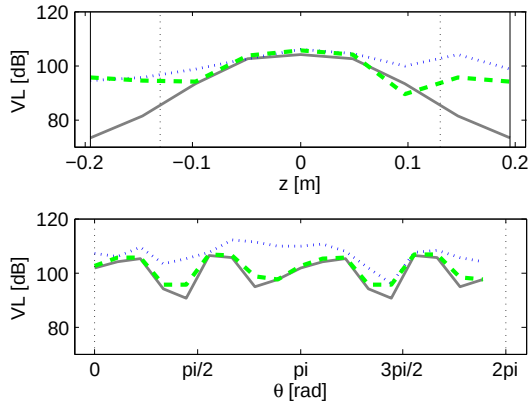

Figure 2.5: Effect of the regularisation procedure on the surface velocity reconstruction along the z axis at $\theta = 0.35$ rad (top) and along the circumference at $z = 0$ m (bottom). Legend: real velocity distribution (solid gray), NAH not regularised (dotted blue), NAH regularised with Tikhonov and GCV (thick dashed green). The graphs refer to $f = 1200$ Hz. The vertical black lines in the top figure help to visualize the geometry: the dotted line represent the limit of the source, while the solid lines are the longitudinal limits of the hologram.

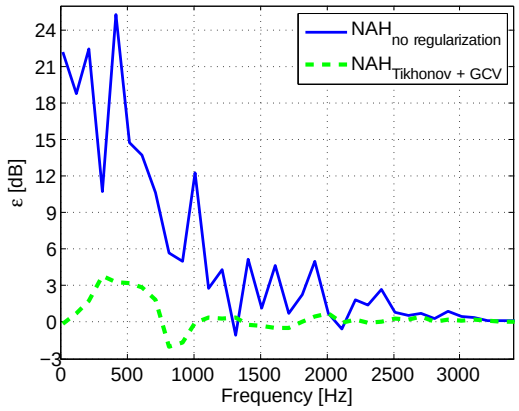

Figure 2.6: ε from 10 to 3410 Hz and step 100 Hz. $d = 0.04$ m and $\Delta \approx 0.05$ m. NAH not regularised (dashed green), and NAH regularised with Tikhonov and GCV (solid blue).

To limit the influence of this phenomenon, the hologram has to be sufficiently long and sufficiently close to the surface of the source, to keep the replicated sources far from the real source. It is consequently important that the microphones which are located nearby the two ends of the hologram measure a much lower pressure than the ones in the central part. On top of this, the hologram distance has to be set as small as possible also in order to detect the exponential decaying evanescent waves. A distance of 0.04 m has been chosen here.

Fig. 2.7 shows the influence of the hologram length, for a fixed hologram distance and spatial sampling. With the exception of the shortest length, all other curves oscillate within

3 dB at low frequency, and become very small above 1500 Hz. Since the results with a hologram of 1.5 times the length of the source are judged accurate enough, this length has been chosen as reference for the simulations, limiting the number of microphones.

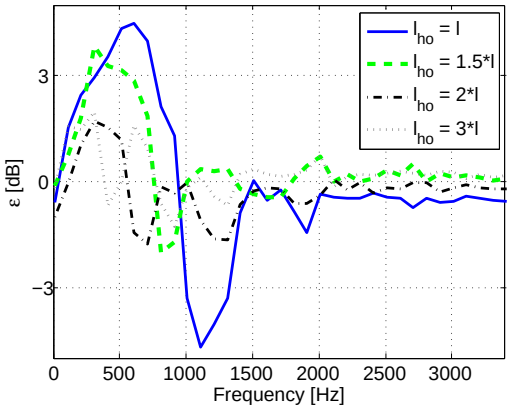

Figure 2.7: ε for four different hologram lengths, from 10 to 3410 Hz and step 100 Hz. $d = 0.04$ m and $\Delta \approx 0.05$ m. l_{ho} and l are the lengths of the hologram and the source, respectively.

5.3.2 Hologram positioning error

A certain level of accuracy characterises the position of the sensors. Stochastic and systematic positioning errors are distinguished and discussed here.

Stochastic errors are due to the accuracy that can be achieved while aligning the acoustic center of the pressure transducers with their theoretical positions on the holographic lattice. This type of error can be effectively corrected by Tikhonov regularisation with GCV (see subsection 3.1).

Furthermore, systematic errors add to the above-mentioned stochastic uncertainty, and consist of centering and alignment errors of the global array as well as its deviation from the circular cross section. Clearly, the regularisation algorithm is not able to filter this type of error [6].

First, some simulations aim to show how much stochastic errors influence the reconstruction of an acoustic source. Fig. 2.8 shows the spatial averaged square error for a normal positioning error with standard deviation $\sigma_{xyz} = 3, 6, 9$ mm on each Cartesian axis. The error introduced by last two positioning inaccuracies (6 and 9 mm) starts deviating from the first case at approximately 2000 Hz. This is justified by the fact that a given positioning error has a stronger influence on a shorter wavelength. Nevertheless, the Tikhonov regularised holography gives acceptable results.

Further simulations have been carried out to investigate the effects of the three types of systematic error, *i.e.*, a global translation of the entire array of 5 mm in all the three Cartesian axes (Fig. 2.9a), an angular misalignment of 0.01 rad of the longitudinal hologram axis (max displacement of 5 mm, Fig. 2.9b), and a stretching of the circular cylinder section to an oval section (max displacement of 5 mm, Fig. 2.9c). A further simulation has been carried out for the sum of all those systematic errors. Fig. 2.10 shows the results. A part from a few

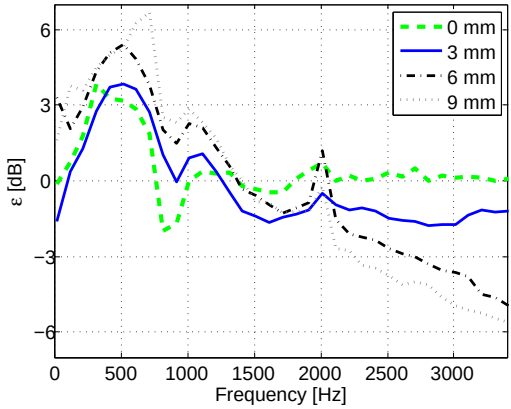

Figure 2.8: Effect of stochastic microphone positioning error for Tikhonov regularised NAH. Spatial averaged square error from 10 to 3410 Hz and step 100 Hz. The values in the legend refer to σ_{xyz}.

outliers and the high frequency range, the errors introduced by this type of inaccuracies are very small or can even be neglected.

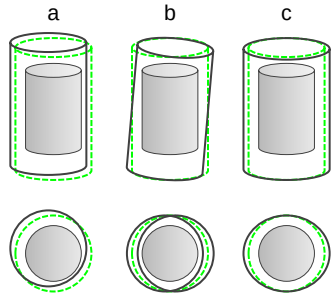

Figure 2.9: Systematic errors. Ideal holograms (dashed green) and geometric errors (solid black).

5.3.3 Measurement noise

A certain amount of noise will always affect the measurements. Two types of noise are discussed here.

The first aspect is environmental background noise. For example, an acoustic source located outside the microphone antenna may introduce a spatially correlated error which cannot be filtered by the regularisation. A typical situation is a wave reflection on a wall. Free-field conditions are needed to avoid this disturbance, which can be achieved in an anechoic room.

A further type of noise is the stochastic electronic noise of the measurement chain. Fig. 2.11 shows a set of simulations which has been performed to investigate this noise source. A normally distributed error has been added to the microphones, with a standard deviation of

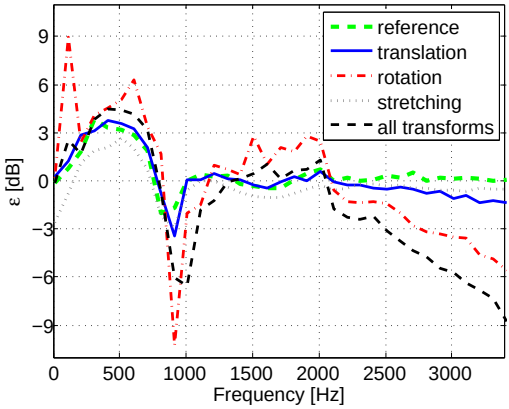

Figure 2.10: NAH spatial averaged square error regularised with Tikhonov and GCV from 10 to 3410 Hz and step 100 Hz. Effects caused by systematic errors.

$0.25, 0.5, 1$ and 3 dB. The figure shows that the Tikhonov regularisation can effectively filter this type of noise (it has a spatially uncorrelated shape with an extremely low magnitude).

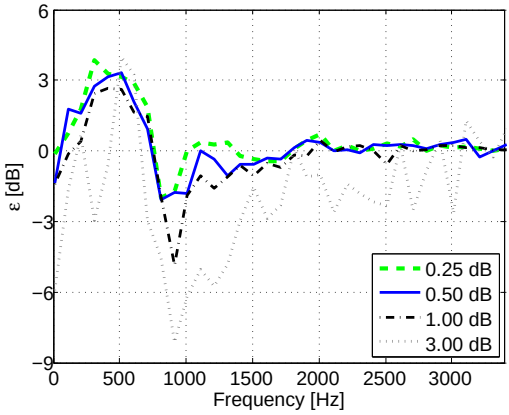

Figure 2.11: NAH spatial averaged square error regularised with Tikhonov and GCV from 10 to 3410 Hz and step 100 Hz. Effects caused by environmental noise.

6 NAH WITH COMPRESSIVE SENSING: NUMERICAL EXPERIMENTS

This section is based on reference [14], and it presents a set of numerical experiments with the aim of investigating compressive sensing within a NAH scheme.

6.1 Test case

A simplified numerical test case has been developed. The test case is one-dimensional, *i.e.*, limited to a cross section of an infinite cylinder. This implies that $k_z = 0$, which corresponds to an infinite wavelength in the longitudinal direction. Moreover, there is no spectral leakage, because the hologram consist of a circumference, along which the signal is periodic.

The dictionary is a complete (orthogonal) Fourier dictionary, built such that eq. (2.13) is satisfied. Accordingly, the source velocity profile is built by 1 or 2 Fourier components, corresponding to a sparsity of 2 and 4, respectively (each Fourier component has two complex conjugate non-zero elements). Finally, no noise is being introduced in the system, and the exact solution is sought.

The source radiates in air, and a single frequency ($f = 5000$ Hz) is considered. Two Fourier components corresponding to a circumferential order of 8 and 18 are taken into account. They refer to a propagating wave and an evanescent wave, respectively. This can be seen looking at the propagators in Fig. 2.1, which have been evaluated under the same settings.

The number of measurement points is $m = 14$, always below Nyquist-Shannon limit (order 8 would need at least 16 points). Moreover, three different sets of transducer positioning are considered. One set consist of regularly spaced microphones, while the other two sets are built from two different random distributions.

Like the example of the classical cylindrical NAH presented in section 5, the source radius is $a = 0.10$ m. Two hologram distances $d = 0.02$ m and $d = 0.04$ m are tested.

Fig. 2.12 shows the source geometry and the velocity distribution. The source consist of 42 points, regularly spaced along a circumference. Such discretization allows to propagate circumferential orders up to the 20$^{\text{th}}$, as indicated by the DFT of the source velocity profile (Fig. 2.12 bottom right).

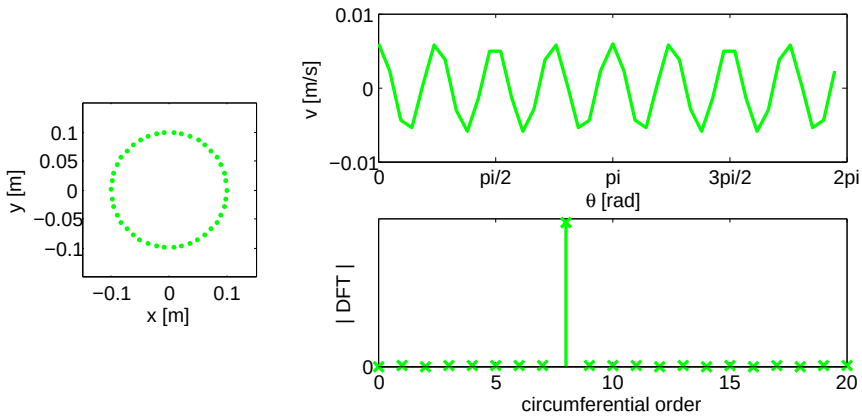

Figure 2.12: Source of the test case: geometry (left), velocity distribution (top right) and its DFT (bottom right).

Fig. 2.13 shows the microphones, according to a regular positioning (circles) and to one random scheme (diamonds), at a distance $d = 0.02$ m. A complex hologram is created starting from the source velocity profile shown in Fig. 2.12. As expected, the evanescent

order 18 is strongly attenuated.

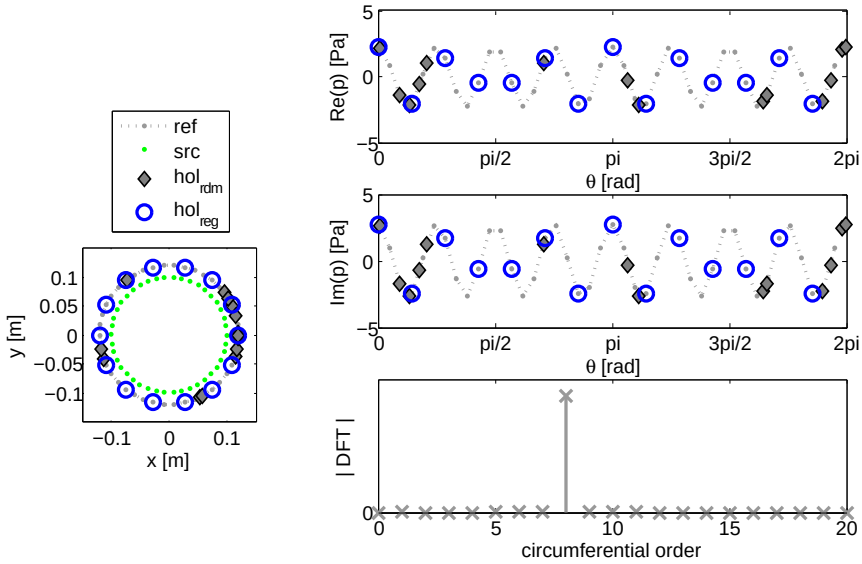

Figure 2.13: Hologram of the test case: microphone positions (left), complex hologram and its DFT (right). Legend: ref is the reference hologram, *i.e.*, the hologram evaluated at the 42 points that correspond to the source points, marked as src; hol_{rdm} and hol_{reg} are the holograms with random and regular spacing, respectively.

6.2 Simulations

6.2.1 Reference scenario

Fig. 2.14 shows the NAH results for a first simulation, which will act as reference scenario for the examples that will be described in the next subsection. Its settings are in line with Fig. 2.12 and 2.13, with the only difference that the evanescent order is omitted. Consequently, only the propagating order 8 is present (sparsity $K = 2$). It can be seen that the reconstruction of the source velocity distribution (thick dashed green) is excellent for both holograms (random and regular positioning are represented by diamonds and circles, respectively). Moreover, in this particular case basis pursuit gives the correct result also for the regularly spaced hologram with sub-Nyquist sampling.

The results have been obtained with a free MATLAB-compatible package called *cvx* [28], which allows for a fully customizable definition of problem and constraints.

6.2.2 Further scenarios

Starting from the reference scenario, three further simulation cases will be presented here.

1. Same as the reference scenario (*i.e.*, $d = 0.02$ m), but including the evanescent order 18 (such that now both orders 8 and 18 are present, with a sparsity $K = 4$). Fig. 2.15 shows again an excellent reconstruction of the velocity profile, but this time only with

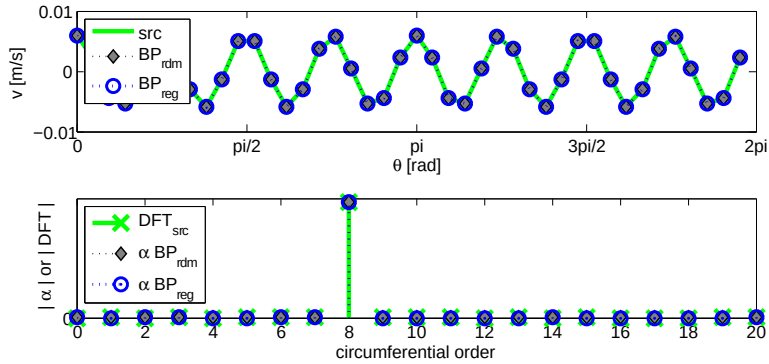

Figure 2.14: Reference scenario: reconstruction of the source velocity distribution (top) and its basis functions (bottom). Legend: src is the source, BP_{rdm} and BP_{reg} are the basis pursuit solutions with random and regular spacing, respectively; DFT_{src} is the amplitude of the source Fourier components, and α are the basis functions obtained through the basis pursuit algorithm.

the randomly spaced hologram. The failure of the regularly spaced hologram is understandable, because the number of microphones is now much below the Nyquist-Shannon limit.

2. Same as point 1 (*i.e.*, $d = 0.02$ m, orders 8 and 18, sparsity $K = 4$), but with a different random positioning. Fig. 2.16 shows that the new set does not allow for a correct source characterisation. This means that point 1 was just a "lucky case" in which basis pursuit gave the correct result.

3. Same as point 1 (*i.e.*, "lucky" random positioning, orders 8 and 18, sparsity $K = 4$), but with a higher distance $d = 0.04$ m. It is clear from Fig. 2.17 that NAH with basis pursuit failed, even if the random set is the one that has previously given the correct results. An increase in the hologram distance reduces the evanescent component substantially. At a certain point, the basis pursuit algorithm it is not able to recognize that component, even if the only noise present is extremely small (the system is affected only by numerical noise). In comparison to classical NAH, holography based on basis pursuit is more sensitive to the problem related to noise and evanescent components.

Those scenarios have been presented in order to show that indeed compressive sensing can give the correct results with less transducers, but at the same time it is extremely dangerous to rely on the solution of NAH with compressive sensing without taking care of the mathematical background, even if the sparsity of the system is very good.

7 CONCLUSIONS

The first part of this chapter gave an overview on Nearfield Acoustical Holography (NAH) in cylindrical coordinates, together with the description of a regularisation scheme. Such approach is well suited for the acoustic characterization of an electric traction motor for green mobility. Moreover, compressive sensing (CS) has been discussed as a possible tool to reduce the number of microphones required by classical NAH in the high frequency range.

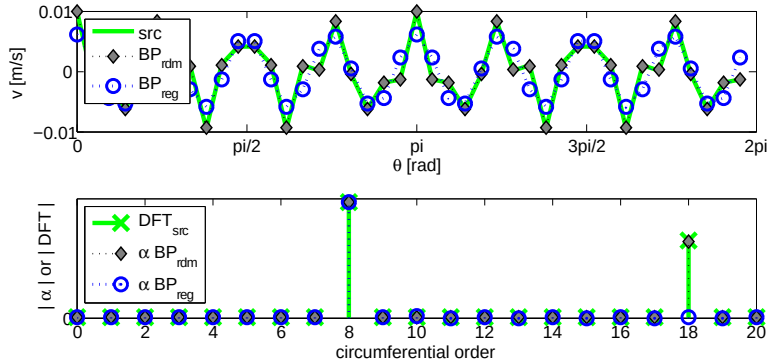

Figure 2.15: Scenario 1: reconstruction of the source velocity distribution (top) and its basis functions (bottom).

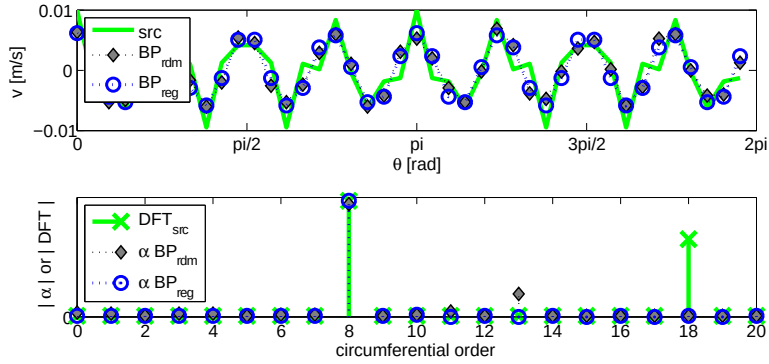

Figure 2.16: Scenario 2: reconstruction of the source velocity distribution (top) and its basis functions (bottom).

A set of numerical simulations showed a few practical aspects of classical cylindrical NAH, and confirmed the results obtained in a previous study [2, 3] for a different geometry.

The proposed antenna layout allows for microphone positioning errors up to 6 mm without introducing substantial errors ($\varepsilon \leq 3$ dB) provided the Tikhonov regularisation combined with a Generalised Cross Validation parameter selection criterion is employed.

The hologram length shall exceed the source longitudinal dimension by a factor of at least 1.5. Specifically, a hologram suitable for studying the acoustic emissions of a cylindrical source with a radius of 0.1 m and a length of 0.3 m up to a frequency of 3400 Hz is a cylindrical structure of radius 0.17 m and length 0.45 m, containing 220 microphones.

A second set of numerical simulations involved a one-dimensional numerical test-case that has been introduced in order to show the applicability of compressive sensing.

Compressive sensing relies on a matrix condition called restricted isometry property (RIP) which, unfortunately, cannot be verified for arbitrary matrices. The RIP does not hold for NAH applications, because of the structure of the matrices that build the system. In particular, the propagators of the wavenumber spectrum (k-space) deteriorate the situation, especially when the different amplification of propagating and evanescent waves becomes

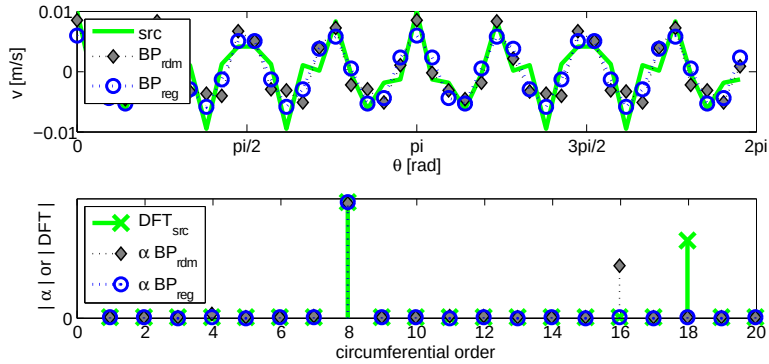

Figure 2.17: Scenario 3: reconstruction of the source velocity distribution (top) and its basis functions (bottom).

substantial. For this reason, a randomisation of the measurement positions cannot lead to a good RIP.

NAH with CS remains promising only if the sparsity of the acoustic field is sufficiently known, and this can be very problematic. To apply compressive sensing within a NAH framework, a good *a priori* knowledge of the source is needed, in order to evaluate the sparsity and enhance it by choosing the most suited dictionary.

REFERENCES

[1] Earl G. Williams. *Fourier Acoustics: Sound Radiation and Nearfield Acoustical Holography*. Academic Press, 1999.

[2] M. Kirchner and E. Nijman. Nearfield acoustical holography for the characterization of cylindrical sources: practical aspects. In *8th International Styrian Noise, Vibration & Harshness Congress (ISNVH 2014), Graz, Austria*, 2014.

[3] M. Kirchner and E. Nijman. *Automotive NVH Technology*, chapter 4 – Cylindrical Nearfield Acoustical Holography: Practical Aspects and Possible Improvements, pages 47–62. SpringerBriefs in Applied Sciences and Technology – Automotive Engineering: Simulation and Validation Methods. Springer, 2016.

[4] Finn Jacobsen and Yang Liu. Near field acoustic holography with particle velocity transducers. *The Journal of the Acoustical Society of America*, 118(5):3139–3144, 2005.

[5] Franançois Ollivier, Sylvie Le Moyne, and Christophe Picard. Experimental comparison of pu probes and microphone arrays used in impulse acoustic holography. In *Proceedings of 14th International Congress on Sound & Vibration (ICSV14), Cairns, Australia*, July 9-12, 2007.

[6] Per Christian Hansen. *Rank-Deficient and Discrete Ill-Posed Problems: Numerical Aspects of Linear Inversion*. SIAM, 1998.

[7] P. A. Nelson and S.H. Yoon. Estimation of acoustic source strength by inverse methods: Part i, conditioning of the inverse problem. *Journal of Sound and Vibration*, 233(4):639 – 664, 2000.

[8] S.H. Yoon and P. A. Nelson. Estimation of acoustic source strength by inverse methods: Part ii, experimental investigation of methods for choosing regularization parameters. *Journal of Sound and Vibration*, 233(4):665 – 701, 2000.

[9] Earl G. Williams. Regularization methods for near-field acoustical holography. *The Journal of the Acoustical Society of America*, 110(4):1976–1988, 2001.

[10] Gilles Chardon, Laurent Daudet, Antoine Peillot, Franois Ollivier, Nancy Bertin, and Rmi Gribonval. Near-field acoustic holography using sparse regularization and compressive sampling principles. *The Journal of the Acoustical Society of America*, 132(3):1521–1534, 2012.

[11] R.G. Baraniuk. Compressive sensing [lecture notes]. *Signal Processing Magazine, IEEE*, 24(4):118–121, July 2007.

[12] E.J. Candes and M.B. Wakin. An introduction to compressive sampling. *Signal Processing Magazine, IEEE*, 25(2):21–30, March 2008.

[13] Brian Hayes. The best bits. In *American Scientist*, volume 97, pages 276–280, July-August 2009.

[14] M. Kirchner and E. Nijman. Cylindrical nearfield acoustical holography using compressive sampling: feasibility and numerical examples. In P. Sas, D. Moens, and H. Denayer, editors, *Proceedings of ISMA2014 including USD2014, Leuven, Belgium*, pages 1531–1546, 15-17 September 2014.

[15] Scott Shaobing Chen, David L. Donoho, and Michael A. Saunders. Atomic decomposition by basis pursuit. *SIAM Rev.*, 43(1):129–159, January 2001.

[16] E.J. Candes and T. Tao. Decoding by linear programming. *Information Theory, IEEE Transactions on*, 51(12):4203–4215, Dec 2005.

[17] E.J. Candes, J. Romberg, and T. Tao. Robust uncertainty principles: exact signal reconstruction from highly incomplete frequency information. *Information Theory, IEEE Transactions on*, 52(2):489–509, Feb 2006.

[18] D.L. Donoho. Compressed sensing. *Information Theory, IEEE Transactions on*, 52(4):1289–1306, April 2006.

[19] D.L. Donoho and J. Tanner. Thresholds for the recovery of sparse solutions via l1 minimization. In *Information Sciences and Systems, 2006 40th Annual Conference on*, pages 202–206, March 2006.

[20] Shaobing Chen and D. Donoho. Basis pursuit. In *Signals, Systems and Computers, 1994. 1994 Conference Record of the Twenty-Eighth Asilomar Conference on*, volume 1, pages 41–44 vol.1, Oct 1994.

[21] Emmanuel J. Candes, Justin K. Romberg, and Terence Tao. Stable signal recovery from incomplete and inaccurate measurements. *Communications on Pure and Applied Mathematics*, 59(8):1207–1223, 2006.

[22] Emmanuel J. Candes. The restricted isometry property and its implications for compressed sensing. *Comptes Rendus Mathematique*, 346(910):589 – 592, 2008.

[23] M. Aharon, M. Elad, and A. Bruckstein. k -svd: An algorithm for designing overcomplete dictionaries for sparse representation. *Signal Processing, IEEE Transactions on*, 54(11):4311–4322, Nov 2006.

[24] J.M. Duarte-Carvajalino and G. Sapiro. Learning to sense sparse signals: Simultaneous sensing matrix and sparsifying dictionary optimization. *Image Processing, IEEE Transactions on*, 18(7):1395–1408, July 2009.

[25] Yinghao Liao, Quan Xiao, Xinghao Ding, and Donghui Guo. A novel dictionary design algorithm for sparse representations. In *Computational Sciences and Optimization, 2009. CSO 2009. International Joint Conference on*, volume 1, pages 831–834, April 2009.

[26] S. Qaisar, R.M. Bilal, W. Iqbal, M. Naureen, and Sungyoung Lee. Compressive sensing: From theory to applications, a survey. *Communications and Networks, Journal of*, 15(5):443–456, Oct 2013.

[27] M. Ochmann. The source simulation technique for acoustic radiation problems. *Acta Acustica united with Acustica*, 81(6):512–527, 1995.

[28] M. Grant and S. Boyd. Graph implementations for nonsmooth convex programs. In V. Blondel, S. Boyd, and H. Kimura, editors, *Recent Advances in Learning and Control*, Lecture Notes in Control and Information Sciences, pages 95–110. Springer-Verlag Limited, 2008.